Authors accepted manuscript: K. Pitt, R.M. Smith, S.A.L. de Koster, J.D. Litster, M.J. Hounslow. Kinetics of immersion nucleation driven by surface tension, Powder Technology 335 (2018) 62-69. Accepted: 1 May 2018. Available online: 1 May 2018.

*Corresponding author: Rachel Smith email: Rachel.smith@sheffield.ac.uk, tel: 01142228255

KINETICS OF IMMERSION NUCLEATION DRIVEN BY SURFACE TENSION

Kate Pitt, Rachel M. Smith*, Stefan A.L. de Koster, James D. Litster & Michael J. Hounslow

University of Sheffield, Sheffield, UK

ABSTRACT

Immersion nucleation is the nuclei formation mechanism for wet granulation systems where the liquid drops are large relative to the primary particles. The process of immersion nucleation has been examined in many studies, however the kinetics of nuclei formation are not well understood, and there is a distinct lack of experimentally validated models for this process.

A kinetic model has been proposed by Hounslow et al. (2009) which describes surface tension driven immersion nucleation. This paper presents the results from a series of experiments measuring the kinetics of immersion nucleation, and these results are compared with the model predictions. Drops of model liquids (aqueous HPMC solution and silicone oil) are placed on static powder beds of zeolite and lactose. Nuclei granules are carefully excavated at different times and the change in granule mass with time is measured. As predicted by Hounslow et al.'s model, the granule mass increases with the square root of time to a maximum granule size at a time t_{max} after an initial adjustment period. The critical packing factor is shown to be a function of powder properties, and not dependent on the liquid properties. The model captures well the measured effects of liquid and powder properties. However, the kinetics of the nucleation process are much slower than predicted by the model. It is believed this is due to continued percolation of the liquid within the powder bed,

after the liquid drop is fully immersed. This secondary liquid movement may have an important effect on granule growth kinetics, and influence final granule product properties.

1. INTRODUCTION

Nucleation is the first stage in any wet granulation process. In general, nucleation can occur through two different processes: immersion nucleation (also known as penetration nucleation), which occurs when the liquid drop size is large compared to the primary particle size, and distribution nucleation, which occurs when the drops are smaller than the primary particle [1,2]. In immersion nucleation, particles surrounding a drop are drawn into the drop by surface tension or other mechanisms [1,3]. Similarly, nuclei may be formed by penetration of a drop into a static or moving powder bed surface driven by capillary pressure [4,5].

Conceptually, there are two models of immersion granulation which are of particular interest, shown in Figure 1. The first, developed by Hapgood and co-workers [4] (see Figure 1a), assumes that a liquid droplet penetrates into a fixed (i.e. non-moving) bed of particles. This bed is modelled as a network of interconnected, static pores. The contact area between the drop and powder remains constant over the entire period of the penetration of the drop. The second model of interest was developed by Hounslow and co-workers [6], and assumes a spherical drop surrounded by powder (see Figure 1b). This model assumes that particles are drawn into the drop, and that the particles drawn into the drop form a critical packing fraction ϕ_{cp}.

In reality, a range of complicated interactions between powder and liquids have been observed in the literature. Emady et al. [7] showed that penetration of a drop into a powder bed is complex with mechanisms varying from spreading to crater formation to tunnelling depending on the properties of the powder. Hapgood and co-workers [8-11] also showed that the process is strongly dependent on the liquid-powder interaction with complex structures formed when non-wetting liquids are used. The kinetics of the immersion nucleation process can be slow, especially when viscous liquid or semi-solid binders are used [12].

We know that the nucleation process is critical to good liquid distribution and ultimately the whole granulation process. Granule growth rate by coalescence and layering is a very strong function of the liquid to solid ratio in the granules. Therefore, any mal-distribution of liquid will lead to very different growth rates and granule size distributions. However, most models of wet granulation neglect the kinetics of the nucleation process completely.

In the last ten years, several groups have developed multidimensional population balance models of granulation which allow distribution of both granule size and liquid content to be tracked [13-18]. However, while development of models for distribution nucleation have progressed [19-23], good models for immersion granulation are still being developed. Poon et al. [24] incorporated an empirical nucleation model based on the estimated drop penetration time into their multidimensional model. The model is somewhat counter-intuitive with better liquid distribution occurring for systems with the longest penetration time. Hapgood et al. [25] proposed a nucleation model for use on population balances. This model accounts effectively for spray zone geometry through the dimensionless spray flux, but assumes the kinetics of the nucleation process are instantaneous. Further work is needed on the development and validation of nucleation models.

Hounslow et al. [6] proposed a promising kinetic model for immersion nucleation driven by surface tension suitable for inclusion in a population balance framework. However, there is no experimental data available with which to validate this modelling approach, or indeed any nucleation kinetics model.

In this paper, the kinetics of the penetration of single drops into static powder beds are carefully measured. This is first study to explicitly isolate the nucleation rate process and experimentally study the dynamic volumes of the nuclei. Both binder and powder properties are also measured. We use these experiments to critically analyse the kinetic model of Hounslow et al. and draw inferences about the kinetics of liquid distribution in a real granulator.

2. IMMERSION NUCLEATION MODEL

Hounslow's model proposed two mechanisms by which particles are immersed in a drop to form a nucleus granule: capillary action driven by surface tension, and diffusion immersion driven by collisions. In this paper, our experiments are performed on a static bed so there is no diffusive element and only capillary driven immersion is considered. The model proposes that particles are drawn into a spherical drop from all sides so that at some intermediate time there is a liquid core surrounded by a layer of immersion particles at some critical-packing liquid volume fraction ϕ_{cp}. The driving force for immersion is the capillary pressure and viscous drag resists the process. The time at which the particles penetrate to the centre of the drop is denoted as t_{max}.

The nucleation model gives the volume of the granule nucleus v as a function of the volume of the liquid drop v_L, the time *t* and properties of the powder:

$$v = \begin{cases} v_L \left(1 + \frac{1-\phi_{cp}}{\phi_{cp}} \sqrt{\frac{t}{t_{max}}}\right) & t \le t_{max} \\ v_L \left(1 + \frac{1-\phi_{cp}}{\phi_{cp}}\right) & t > t_{max} \end{cases} \qquad \textit{Eq (1)}$$

where

$$t_{max} = \frac{18.75\mu h_0^2}{\gamma^{lv} cos\theta d_p} \frac{1-\phi_{cp}^{1/3}}{\phi_{cp}^3} \qquad \textit{Eq (2)}$$

Here, μ is the binder viscosity, h_o is the initial drop size, $\gamma^{lv} cos\theta$ is the adhesive tension of the fluid with respect to the powder and d_p is the primary particle size. We can rewrite Eq.1 in terms of the granule mass for direct comparison with experiment:

$$m_g = \begin{cases} m_L + \left(m_g^* - m_L\right)\left(\frac{t}{t_{max}}\right)^{1/2} & t \le t_{max} \\ m_g^* & t > t_{max} \end{cases} \qquad \textit{Eq (3)}$$

where m_L, m_g and m_g^* are the drop mass, the granule mass and the final granule mass respectively. The dry mass of the granule is simply $m_g - m_L$.

The mechanism described here is very similar to the Washburn equation for the wicking of liquid into a powder bed. Hapgood et al. [4] developed an expression for the drop penetration time into a powder bed based on the Washburn equation. Although the dynamics of the process were not explicitly given, the same dependence of granule size on $t^{1/2}$ is implied. If Hapgood's effective porosity is assumed to be ϕ_{cp}, then it can be shown that her predicted penetration time t_p is closely related to t_{max}:

$$t_{max} = 1.78\frac{\left(1-\phi_{cp}^{1/3}\right)}{\left(1-\phi_{cp}\right)}t_p \qquad \textit{Eq (4)}$$

The slightly different expression is due to the different geometry assumed – spherical for Hounslow or cylindrical for Hapgood. The Hounslow model is probably more physically realistic for the tunnelling regime.

3. METHODS AND MATERIALS

Single drop granule nucleation experiments were conducted to measure granule growth after impact of each binder droplet with a powder bed. In this work, four different powder-binder systems were studied: (i) sodium aluminosilicate (zeolite) – hydroxy propyl methylcellulose (HPMC), (ii) sodium aluminosilicate – silicone oil, (iii) α-lactose monohydrate – hydroxy propyl methylcellulose and (iv) α-lactose monohydrate – silicone oil.

3.1 Material characterisation

Powder properties

Sodium aluminosilicate was supplied from PQ Corporation. α-lactose monohydrate (Pharmatose 200 M) was supplied by DFE Pharma. The properties of the powders are given in Table 1. Particle size analysis was carried out using laser diffraction (Malvern Mastersizer 2000). The volume frequency distribution of particle size in Figure 2 shows the differences in size distributions between the two powders. The true particle density of sodium aluminosilicate was measured using helium pycnometry.

Binder solution properties

Two different binders were used at varying viscosities; (i) silicone oil at three different viscosities and (ii) hydroxyl propyl methylcellulose (HPMC) at five different viscosities. The silicone oils were supplied by Sigma-Aldrich. HPMC (Tylopur®) was supplied by Shin Etsu. In order to aid the identification of the granules within the powder beds, the silicone oil and HPMC solutions were dyed red with Sudan IV (Sigma-Aldrich) and erythrosin B (Sigma-Aldrich) respectively. The binder solution properties for the silicone oils and different concentrations of HPMC are given in Tables 2 and 3 respectively. For the lactose-HPMC experiments, the HMPC solutions were prepared using saturated lactose solutions in order to prevent the dissolution of the lactose powder bed. The properties of the lactose saturated HPMC solutions are given in Table 4. The mass of individual droplets was recorded using a Mettler Toledo UMT2 Ultra-Micro Balance. The liquid-air interfacial tension of pendant droplets and the droplet sizes were measured using a First Ten Angstroms FTA 125 goniometer. The viscosities of the different concentrations of HPMC were measured using a Malvern Kinexus rotational rheometer.

3.2 Experimental method

The powder beds were prepared by lightly sieving the powders through a 1.18 mm sieve into petri dishes, which were subsequently levelled with a plastic ruler to achieve an even surface. A single droplet of binder solution was manually released from a 5 ml syringe which was clamped at either 5 cm or 20 cm above the powder surface. After a certain time interval following droplet contact with the powder bed, the granule was extracted from the powder into a 1 mm sieve using a spatula, with the non-granulated powder falling through the sieve. The granule was subsequently weighed using a Mettler Toledo UMT2 Ultra-Micro Balance. For each experiment, granules were extracted after increasing time intervals until there was no further change in granule mass. For each time interval, the mass of a minimum of ten granules was recorded and the average value taken.

4. RESULTS AND DISCUSSION

Typical results for kinetics of nuclei growth for lactose and zeolite powders with HPMC and silicone oil binders are shown in Figure 3. The change in granule mass with time follows the trend predicted by Eq. 3, i.e. granule mass increases with $t^{1/2}$ until a maximum granule mass is reached at t_{max}. For lactose and HPMC the apparent liquid mass, i.e. the mass of the nucleus extrapolated to $t = 0$ is entirely consistent with the measured droplet mass. This is also true for the low viscosity silicone oil on both powders. For the other systems, however, the apparent mass is substantially higher.

For these powder-binder systems, there are clearly some more complex processes happening in the early stages of the nuclei formation. Collection of data at times shorter than 30 s was not possible, and therefore the effect was not able to be quantified. It is likely that early in the process, the liquid volume fraction is greater than ϕ_{CP} and changing with time. Thus the measured apparent t_{max} is less than the true value at constant ϕ_{CP}. For fair comparison with the model, we calculate t_{max} from the measured apparent value as (see Figure 4):

$$t_{max} = t_{max}^{app}\left(\frac{m_g^* - m_L}{m_g^* - m_L^{app}}\right)^2 \qquad \textit{Eq (5)}$$

Data for all powder combinations is plotted in Figure 5. For all data, Eq. 1 provides an excellent fit to the data. The capillary pressure driven model for granule formation gives an excellent prediction of the nucleation kinetics.

Figure 6 shows the ultimate granule volume as a function of the liquid drop volume for all data. Four groups of points are visible corresponding to the combinations of two solids and two binders. The small droplet volumes are for silicone oil, the larger droplets are HPMC. For each binder, the larger granules are lactose and the smaller zeolite. The ultimate granule volume, and thus ϕ_{cp}, depends only on the solid form, and not on the binder used. The slope of each line is the reciprocal of the critical packing liquid volume fraction ϕ_{cp}. Based on this graph, the values of ϕ_{cp} are 0.564

± 0.010 and 0.256 ± 0.008 for zeolite and lactose respectively. Zeolite particles are porous and liquid captured inside the particles is included in ϕ_{cp}. Therefore, zeolite granules are expected to have a larger liquid volume fraction than non-porous lactose crystals and the values of ϕ_{cp} are reasonable for both materials.

Figure 7 shows the effect of viscosity on t_{max}. As predicted by Eq. 2, t_{max} varies linearly with binder viscosity for both powders with the constant of proportionality depending on the binder/solid pair. Then the theoretical slopes of Figure 7 can be calculated as:

$$\frac{t_{max}}{\mu} = \frac{18.75h_0^2}{\gamma^{lv}cos\theta d_p}\frac{1-\phi_{cp}^{1/3}}{\phi_{cp}^3} \qquad Eq\ (2)$$

given the values of ϕ_{cp} from Figure 6 and the measured values of h_0 and $\gamma^{lv}cos\theta$ for each powder-binder pair (see Section 3.1). Table 5 lists the measured and predicted values for t_{max}/μ for the four powder-binder combinations. While the trends in t_{max}/μ are similar, the measured values are one to two orders of magnitude higher than the predicted values.

Thus, although the model predicts the correct form of the nucleation kinetics, and the correct effect of powder and binder properties, the measured nucleation time is much larger than that predicted by Eqs. 1 to 3. This is a surprising result. Hapgood measured t_p for a wide range of systems with very similar drop size [4]. Hapgood's experiments were based on filmed visual observations of the liquid penetration, and t_p was taken as the time at which the liquid was no longer visible at the surface of the powder bed. Her experiments differ from those presented here, in which the nuclei masses were measured until growth stopped. Her longest measured t_p was 130 s for lactose (d_{32} = *18 μm;* d_{43} = *69 μm)* with 7% HPC solution (μ = *104 mPa.s*). We have a very similar lactose-HPC system with a measured t_{max} of around 780 s. This seems to indicate that there continues to be substantial migration of liquid within the bed after the drop has fully penetrated the bed surface. Nuclei granule mass continues to increase by liquid migrating down fine capillaries

leaving a partially saturated outer shell on the granule. The presence of this partially saturated outer shell has been observed experimentally and is shown conceptually in Figure 8.

5. CONCLUSIONS

In this paper, the kinetics of nuclei formation by penetration of single drops into static powder beds are carefully measured for the first time. In all cases, after an initial adjustment period, the granule mass increases with the square root of time to a maximum granule size at a time t_{max} as predicted by Hounslow et al.'s model. The corresponding critical packing liquid volume fraction is a function of powder type only and calculated values are physically reasonable. The measured effects of primary particle size, liquid viscosity and surface tension on nucleation kinetics are also well predicted by the model. However, the kinetics of the process are one to two orders of magnitude slower than the immersion nucleation model predicts. This implies that there is significant secondary migration of liquid within the bed after the drop had fully penetrated the powder. This secondary nucleation stage may make an important contribution to liquid distribution and granule growth kinetics in granulators.

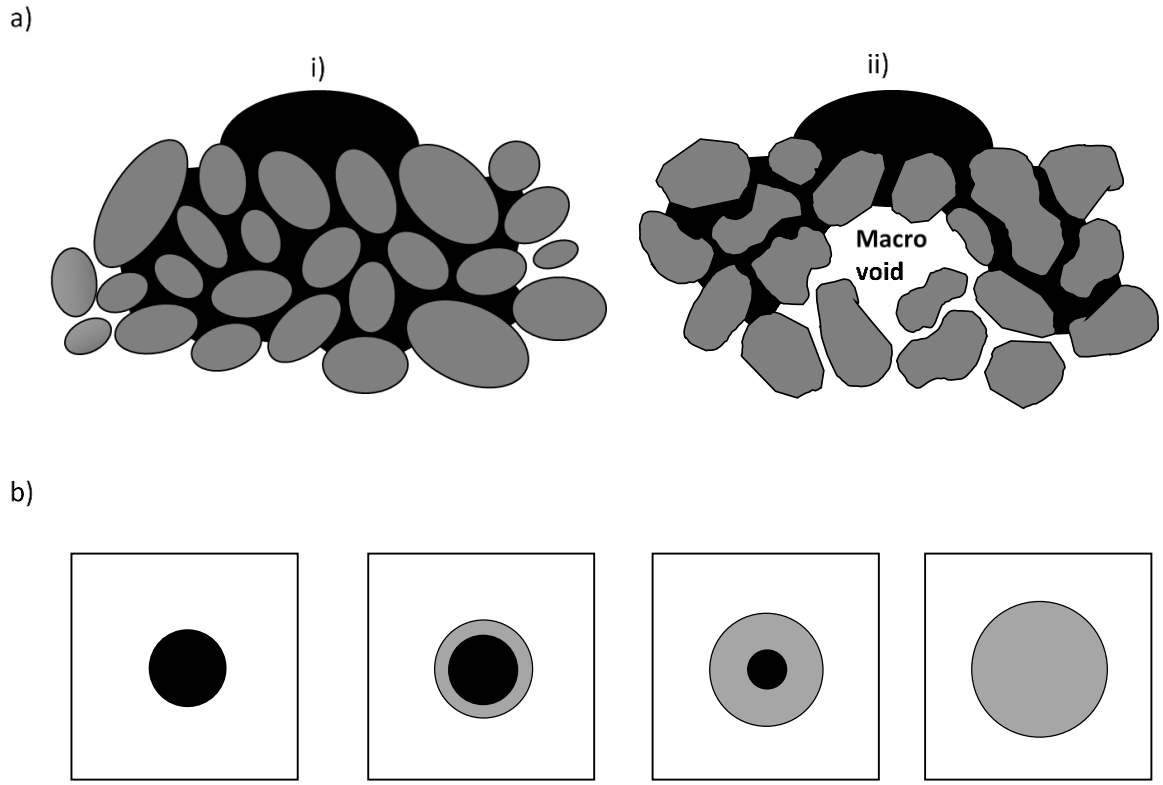

Figure 1. (a) Visual representation of example models for immersion nucleation. a) The Hapgood model, demonstrating the liquid penetration from a droplet into pores with i) random close packing, and ii) irregular packing. Figure adapted from [4]. b) Hounslow's immersion nucleation model, showing an increasing wetted powder fraction (grey) and decreasing liquid droplet size (black) with time. Figure adapted from [6].

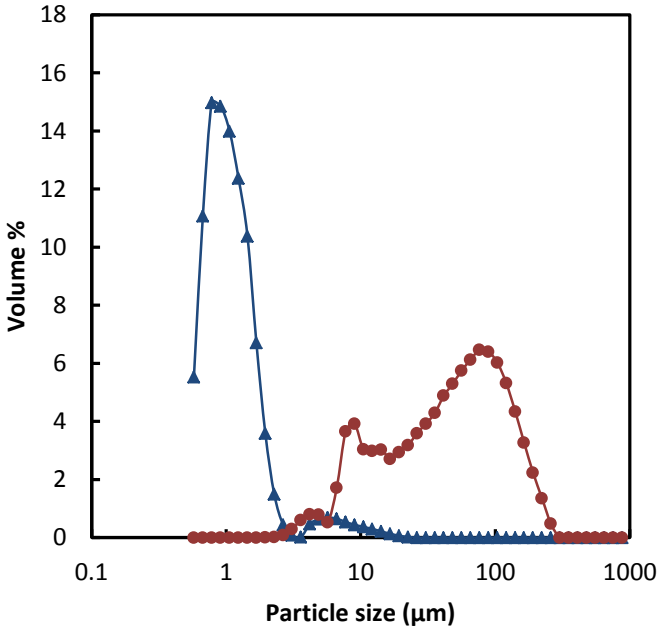

Figure 2. Volume frequency distribution of powders. Triangles represent zeolite. Circles represent lactose.

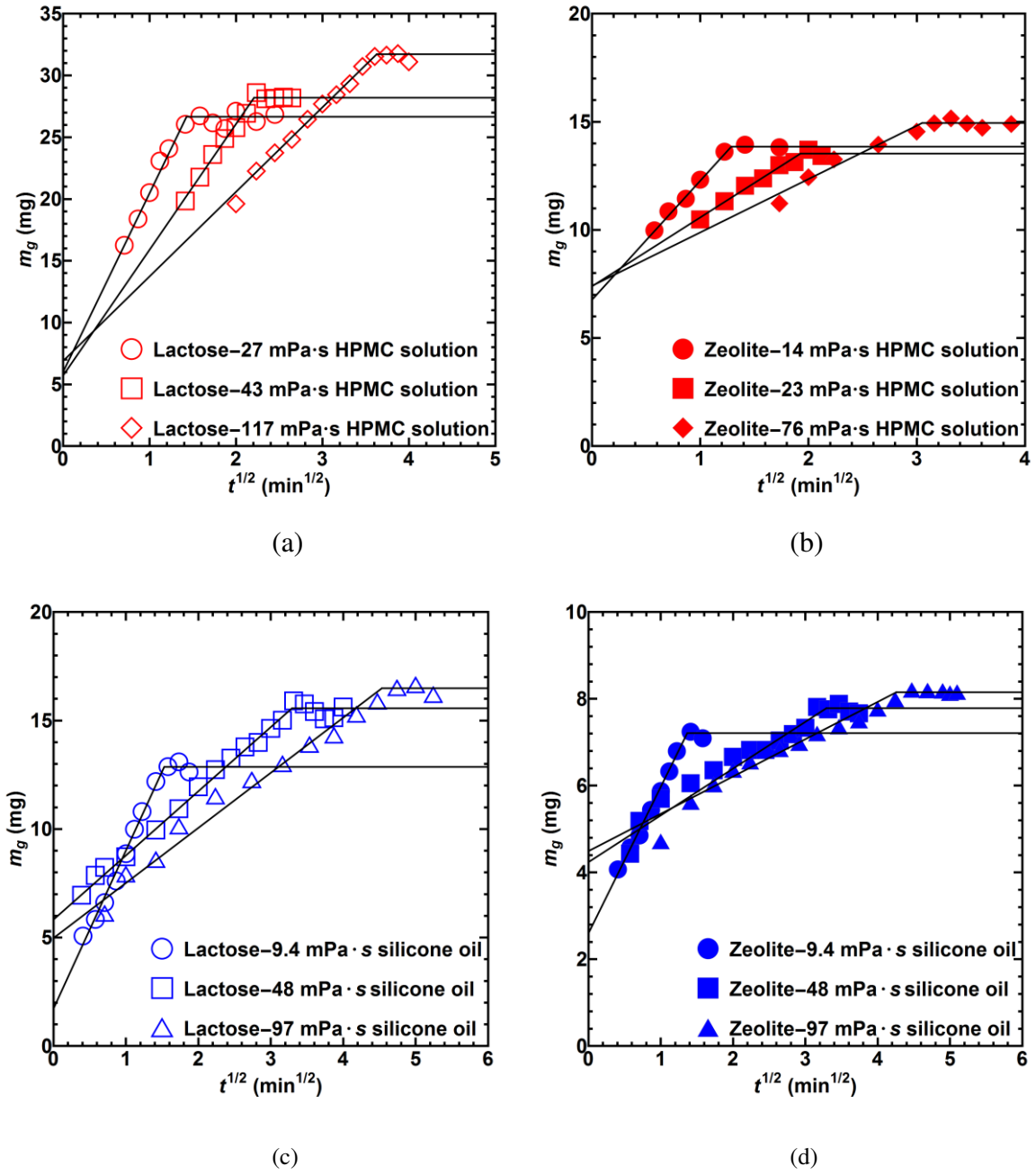

Figure 3. Typical experimental data for (a) lactose and (b) zeolite nuclei bound with different viscosity HPMC solutions. Measured droplet masses were 5.46mg, 5.56mg and 6.19mg respectively; (c) lactose and (d) zeolite bound with different viscosity silicone oil solutions. Measured droplet masses were 1.86mg, 2.15mg and 2.18mg respectively.

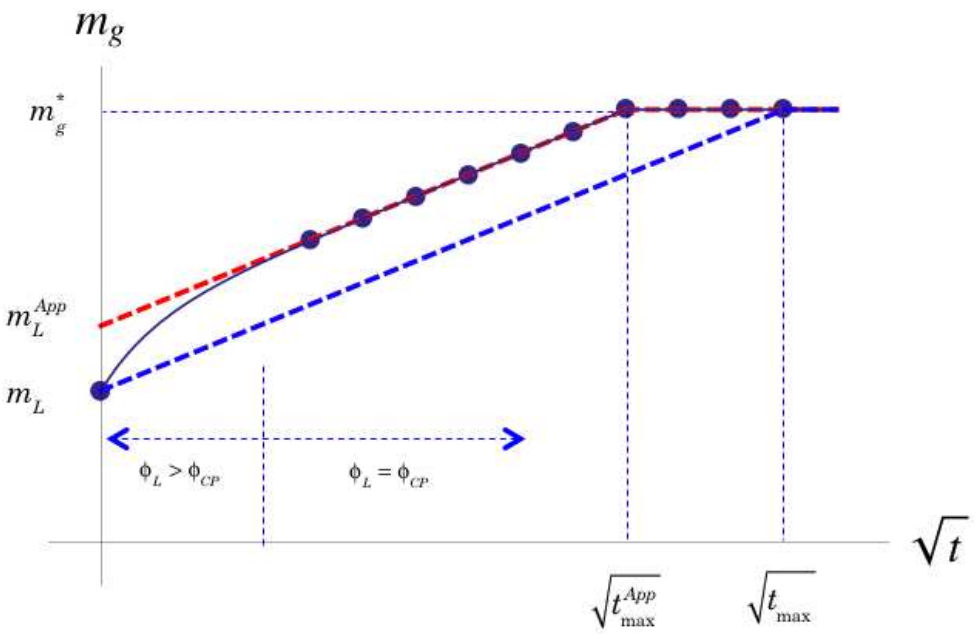

Figure 4. Method to calculate t_{max} for data where the apparent liquid drop mass is substantially different from the true drop mass.

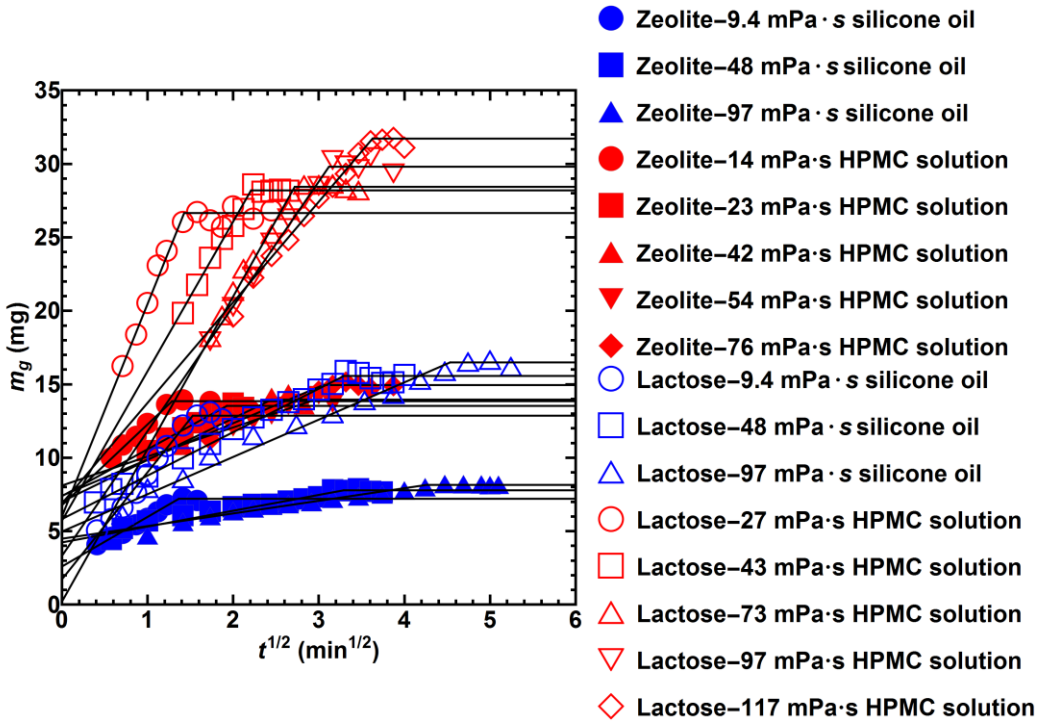

(a)

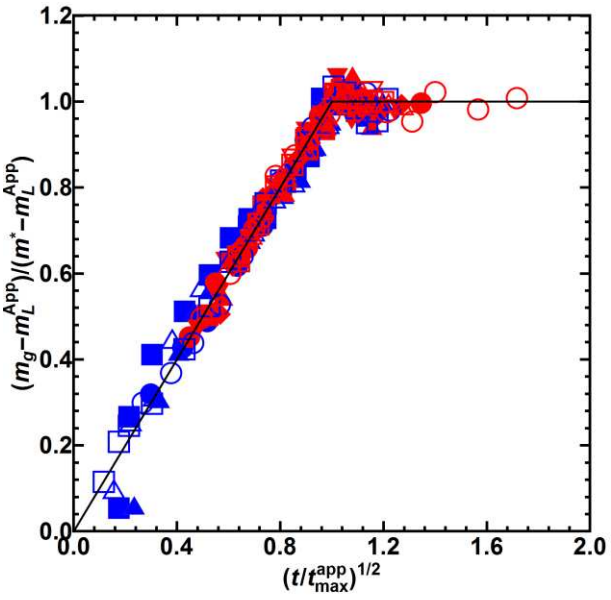

(b)

Figure 5. Nuclei mass of lactose and zeolite with a range of HPMC solutions and silicone oils of different viscosities (a) raw data; (b) data adjusted using Eq. 5. The line in Figure 4(b) is Eq. 1.

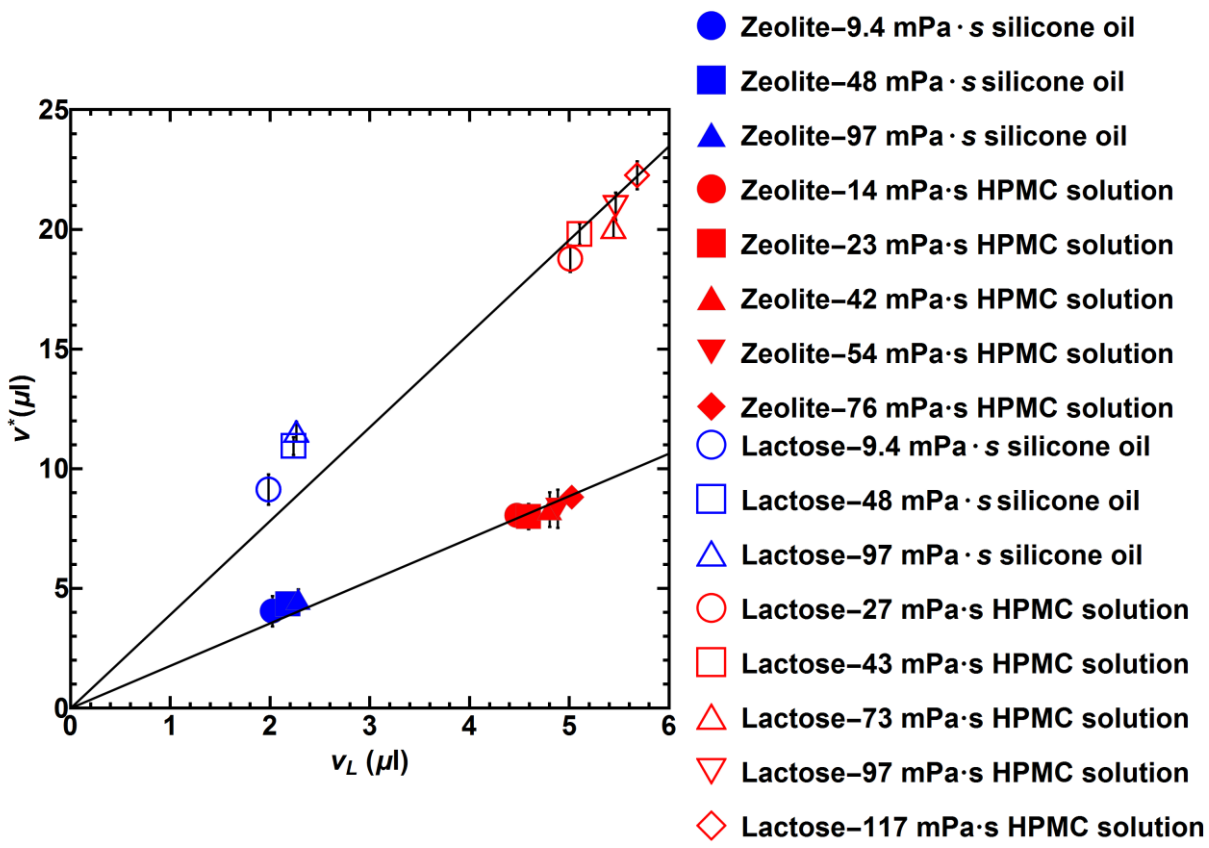

Figure 6. Ultimate granule volume (v*) as a function of droplet volume (v_L). The upper line is for lactose.

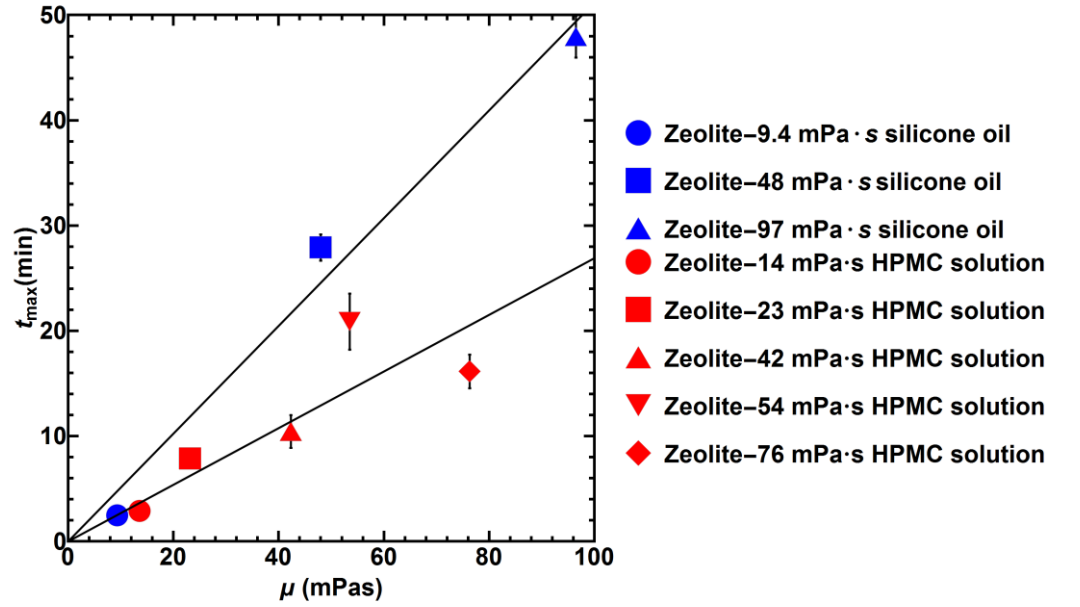

(a)

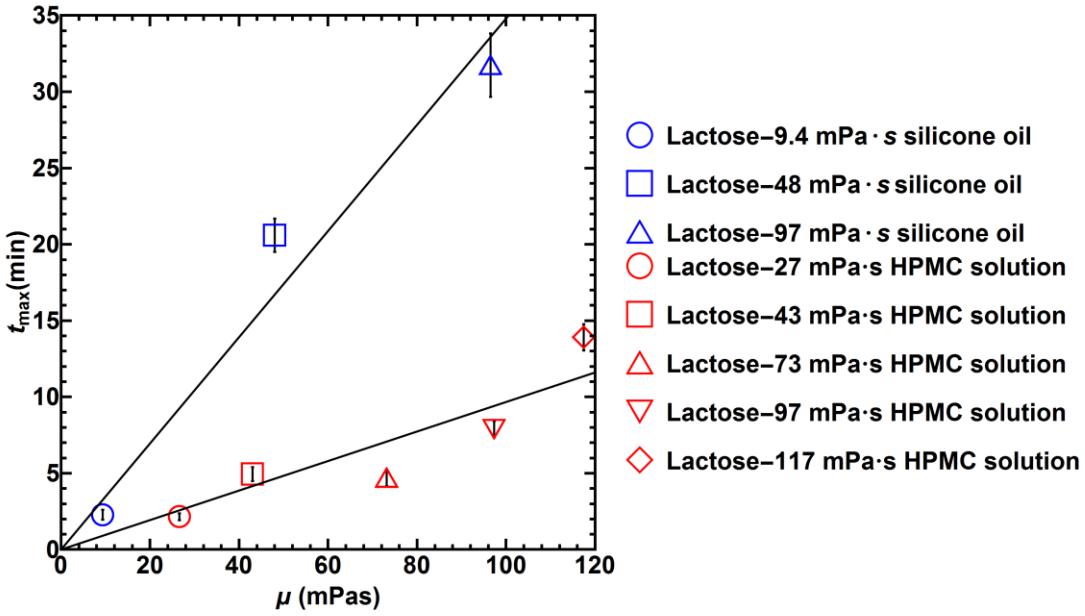

(b)

Figure 7. The effect of binder viscosity on t_{max} for (a) zeolite and (b) lactose. The upper line in both cases is for silicone oil.

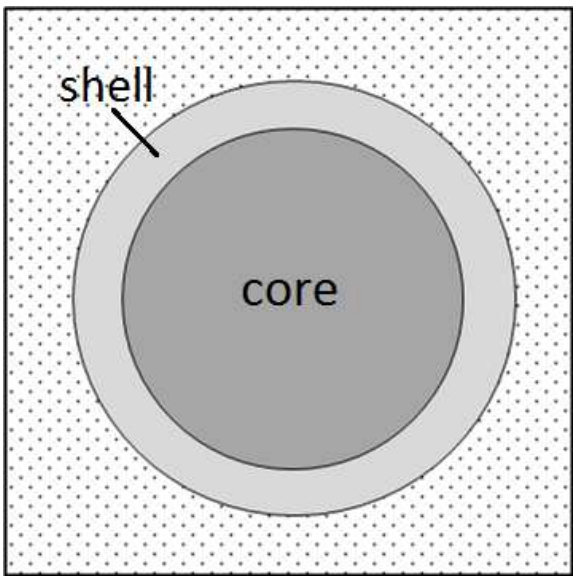

Figure 8. A schematic of the proposed nuclei structure, showing a fully saturated core surrounded by a partially saturated outer powder shell.

	True density (g/cm^3)	Particle size (μm)				
		Surface mean, $d_{3,2}$	Volume mean, $d_{4,3}$	d_{10}	d_{50}	d_{90}
Sodium aluminosilicate	2.11	0.93	1.30	0.62	0.95	1.68
α-lactose monohydrate	1.54*	21.7	57.6	8.15	45.1	127

*Data supplied by DFE pharma

Table 1. Powder properties.

	Density* (g/cm^3)	Viscosity (mPa.s)	Droplet mass (mg)	Droplet diameter (mm)	Interfacial tension* (mN/m)
Silicone oil 10cSt	0.935	9.35	1.86 (0.04)	1.48 (0.01)	20.1
Silicone oil 50cSt	0.960	48.0	2.17 (0.04)	1.52 (0.02)	20.8
Silicone oil 100cSt	0.965	96.5	2.18 (0.06)	1.54 (0.02)	20.9

*Supplied by Sigma Aldrich (at 25˚C)

Table 2. Silicone oil properties (Standard deviations given in brackets).

	Density (g/cm^3)	Viscosity (mPa.s)	Droplet mass (mg)	Droplet diameter (mm)	Interfacial tension (mN/m)
HPMC 6%	1	13.6 (0.6)	4.47 (0.09)	1.94 (0.06)	46.1 (1.5)
HPMC 8%	1	23.2 (1.1)	4.59 (0.08)	1.98 (0.05)	44.3 (1.5)
HPMC 10%	1	42.3 (0.8)	4.80 (0.06)	2.00 (0.05)	44.1 (1.5)
HPMC 11%	1	53.5 (0.3)	4.88 (0.05)	2.02 (0.05)	43.8 (2.9)
HPMC 12%	1	76.3 (0.9)	4.97 (0.06)	2.03 (0.01)	43.1 (2.3)

Table 3. HPMC solution properties (Standard deviations given in brackets).

	Density (g/cm^3)	Viscosity (mPa.s)	Droplet mass (mg)	Droplet diameter (mm)	Interfacial tension (mN/m)
HPMC 6%	1.09	26.6 (1.3)	5.46 (0.07)	1.97 (0.08)	46.4 (1.8)
HPMC 8%	1.09	43.0 (3.3)	5.56 (0.03)	1.98 (0.08)	45.6 (1.5)
HPMC 10%	1.09	73.2 (0.9)	5.93 (0.05)	1.99 (0.09)	44.8 (1.7)
HPMC 11%	1.09	97.3 (4.2)	5.96 (0.09)	2.00 (0.04)	43.0 (2.4)
HPMC 12%	1.09	117 (1)	6.19 (0.06)	2.01 (0.05)	42.9 (1.8)

Table 4. Lactose-saturated HPMC binder solution properties (Standard deviations given in brackets).

	Zeolite measured	Zeolite predicted	Lactose measured	Lactose predicted
Silicone Oil	$31 \pm 2 \times 10^3$	3.87×10^2	$21 \pm 2 \times 10^3$	5.21×10^2
HPMC	$16 \pm 2 \times 10^3$	3.12×10^2	$5.8 \pm 0.7 \times 10^3$	4.21×10^2

Table 5. Measured and predicted values of t_{max}/μ (1/Pa).

LIST OF SYMBOLS

d_p	Primary particle diameter	[m]
h	Nucleus size	[m]
h_0	Drop size	[m]
m_g	Granule mass	[kg]
m_g^*	Ultimate granule mass	[kg]
m_L	Drop mass	[kg]
m_l^{app}	Apparent drop mass	[kg]
t	Time	[s]
t_{max}	Total nucleation time	[s]
t_{max}^{app}	Apparent nucleation time	[s]
t_p	Drop penetration time	[s]
$\gamma^{lv}cos\theta$	Adhesive tension	[N.m]
ϕ_{cp}	Critical liquid packing fraction	[-]
μ	Viscosity	[Pa.s]
v	Volume of granule nucleus	[m^3]
v^*	Ultimate granule volume	[m^3]
v_L	Volume of liquid droplet	[m^3]

ACKNOWLEDGEMENTS

The authors wish to acknowledge financial support from the EPSRC.

REFERENCES

[1] T. Schæfer, C. Mathiesen, Melt pelletization in a high shear mixer. IX. Effects of binder particle size, Int. J. Pharm. 139 (1996) 139-148.

[2] W.I.J. Kariuki, B. Freireich, R.M. Smith, M. Rhodes, K.P. Hapgood, Distribution nucleation: Quantifying liquid distribution on the particle surface using the dimensionless particle coating number, Chem. Eng. Sci., 92 (2013) 134-145.
[3] T. Abberger, A. Seo, T. Schaefer, The effect of droplet size and powder particle size on the mechanisms of nucleation and growth in fluid bed melt agglomeration, Int. J. Pharm. 249 (2002) 185-197.
[4] K.P. Hapgood, J.D. Litster, S.R. Biggs, T. Howes, Drop penetration into porous powder beds, J. Coll. Int. Sci. 253 (2002) 353-366.
[5] K.P. Hapgood, J.D. Litster, R.M. Smith, Nucleation regime map for liquid bound granules, AIChE J., 49 (2003) 350-361.
[6] M.J. Hounslow, M. Oullion, G.K. Reynolds, Kinetic models for granule nucleation by the immersion mechanism, Powder Technol., 189 (2009) 177-189.
[7] H.N. Emady, D. Kayrak-Talay, J.D. Litster, A Regime Map for Granule Formation by Drop Impact on Powder Beds, AIChE J., 59 (2013) 96-107.
[8] K.P. Hapgood, L. Farber, J.N. Michaels, Agglomeration of hydrophobic powders via solid spreading nucleation, Powder Technol., 188 (2009) 248-254.
[9] K.P. Hapgood, B. Khanmohammadi, Granulation of hydrophobic powders, Powder Technol., 189 (2009) 253-262.
[10] N. Eshtiaghi, B. Arhatari, K.P. Hapgood, Producing hollow granules from hydrophobic powders in high-shear mixer granulators, Adv. Powder Technol., 20 (2009) 558-566.
[11] T.H. Nguyen, K. Hapgood, W. Shen, Observation of the liquid marble morphology using confocal microscopy, Chem. Eng. J., 162 (2010) 396-405.
[12] M. Oullion, G.K. Reynolds, M.J. Hounslow, Simulating the early stage of high-shear granulation using a two-dimensional Monte-Carlo approach, Chem. Eng. Sci., 64 (2009) 673-685.
[13] D.A. Pohlman, J.D. Litster, Coalescence model for induction growth behavior in high shear granulation, Powder Technol., 270 (2015) 435-444.
[14] D. Verkoeijen, G.A. Pouw, G.M.H. Meesters, B. Scarlett, Population balances for particulate processes - a volume approach, Chem. Eng. Sci., 57 (2002) 2287-2303.
[15] C.D. Immanuel, F.J. Doyle, Solution technique for a multi-dimensional population balance model describing granulation processes, Powder Technol., 156 (2005) 213-225.
[16] J.M.H. Poon, R. Ramachandran, C.F.W. Sanders, T. Glaser, C.D. Immanuel, F.J. Doyle, J.D. Litster, F. Stepanek, F.Y. Wang, I.T. Cameron, Experimental validation studies on a multi-dimensional and multi-scale population balance model of batch granulation, Chem. Eng. Sci., 64 (2009) 775-786.
[17] L. Madec, L. Falk, E. Plasari, Modelling of the agglomeration in suspension process with multidimensional kernels, Powder Technol., 130 (2003) 147-153.
[18] A. Darelius, H. Brage, A. Rasmuson, I.N. Bjorn, S. Folestad, A volume-based multi-dimensional population balance approach for modelling high shear granulation, Chem. Eng. Sci., 61 (2006) 2482-2493.
[19] F. Stepanek, P. Rajniak, C. Mancinelli, R.T. Chern, R. Ramachandran, Distribution and accessibility of binder in wet granules, Powder Technol., 189 (2009) 376-384.
[20] K. Terrazas-Velarde, M. Peglow, E. Tsotsas, Stochastic simulation of agglomerate formation in fluidized bed spray drying: A micro-scale approach, Chem. Eng. Sci., 64 (2009) 2631-2643.
[21] K. Terrazas-Velarde, M. Peglow, E. Tsotsas, Investigation of the Kinetics of Fluidized Bed Spray Agglomeration Based on Stochastic Methods, AIChE J., 57 (2011) 3012-3026.
[22] M. Hussain, J. Kumar, M. Peglow, E. Tsotsas, Modeling spray fluidized bed aggregation kinetics on the basis of Monte-Carlo simulation results, Chem. Eng. Sci., 101 (2013) 35-45.
[23] M. Hussain, M. Peglow, E. Tsotsas, J. Kumar, Modeling of Aggregation Kernel Using Monte Carlo Simulations of Spray Fluidized Bed Agglomeration, AIChE J., 60 (2014) 855-868.
[24] J.M.H. Poon, C.D. Immanuel, F.J. Doyle, J.D. Litster, A three-dimensional population balance model of granulation with a mechanistic representation of the nucleation and aggregation phenomena, Chem. Eng. Sci., 63 (2008) 1315-1329.
[25] K.P. Hapgood, J.D. Litster, E.T. White, P.R. Mort, D.G. Jones, Dimensionless spray flux in wet granulation: Monte-Carlo simulations and experimental validation, Powder Technol., 141 (2004) 20-30.